Multi-instrumental analysis of large sprite events and their producing storm in southern France

S. Soula [a,*], F. Iacovella [a], O. van der Velde [b], J. Montanyà [b], M. Füllekrug [c], T. Farges [d], J. Bór [e], J.-F. Georgis [a], S. NaitAmor [f], J.-M. Martin [a]

[a] *Laboratoire d'Aérologie, Université de Toulouse/CNRS, Toulouse, France*
[b] *Electrical Engineering Department, Technological University of Catalonia, Terrassa, Spain*
[c] *Department of Electronic and Electrical Engineering, University of Bath, Bath, United Kingdom*
[d] *CEA, DAM, DIF, F-91297 Arpajon, France*
[e] *Geodetic and Geophysical Institute, Research Centre for Astronomy and Earth Sciences, Hungarian Academy of Sciences, Sopron, Hungary*
[f] *CRAAG, Algiers, Algeria*

ABSTRACT

During the night of 01-02 September, 2009, seventeen distinct sprite events including 3 halos were observed above a storm in north-western Mediterranean Sea, with a video camera at Pic du Midi (42.93N; 0.14E; 2877 m). The sprites occurred at distances between 280 and 390 km which are estimated based on their parent CG location. The MCS-type storm was characterized by a trailing-stratiform structure and a very circular shape with a size of about 70,000 km^2 (cloud top temperature lower than -35 °C) when the TLEs were observed. The cloud to ground (CG) flash rate was large (45 min^{-1}) one hour before the TLE observation and very low (<5 min^{-1}) during it. Out of the 17 sprite events, 15 parent +CG (P+CG) strokes have been identified and their average peak current is 87 kA (67 kA for the 14 events without halo), while the associated charge moment changes (CMC) that could be determined, range from 424 to 2088±20% C km. Several 2-second videos contain multiple sprite events: one with four events, one with three events and three with two events. Column and carrot type sprites are identified, either together or separately. All P+CG strokes are clearly located within the stratiform region of the storm and the second P+CG stroke of a multiple event is back within the stratiform region. Groups of large and bright carrots reach ~70 km height and ~80 km horizontal extent. These groups are associated with a second pulse of electric field radiation in the ELF range which occur ~5 ms after the P+CG stroke and exhibits the same polarity, which is evidence for current in the sprite body. VLF perturbations associated with the sprite events

were recorded with a station in Algiers.

1. Introduction

For several years in the frame of Eurosprite program, campaigns for TLEs observations are organized in southern Europe. Numerous sprites and other TLEs have been observed above thunderclouds which regularly develop from the beginning of May to the end of November (Neubert et al., 2005, 2008; van der Velde et al., 2006; Soula et al., 2009, 2010). The typical characteristics of TLEs determined in other regions of the world are also observed in the cases detected in southern and central France for the summer season, and along the Mediterranean coastline for the fall season. The sprites occur over mesoscale convective systems (MCSs) rapidly after a positive cloud-to-ground (+CG) flash (Boccippio et al., 1995; Sentman et al., 1995; Lyons, 1996; Pasko et al., 1997; Hayakawa et al., 2004) and the elves occur more frequently above storms over sea (Chen et al., 2008). Case studies in Europe allowed distinguishing some relationships between sprite type and delay of production after the parent CG flash (van der Velde et al., 2006) and specifics of the lightning activity associated with sprite production and CG flash sequences (Soula et al., 2010). Among different mechanisms proposed to explain sprite generation, the heating of ambient electrons by quasi-electrostatic (QE) fields above the storm is considered to be the most likely (e.g. Pasko et al., 1997).

Electromagnetic radiations associated with TLEs have been recorded in several cases of observations. For Gigantic Jets (GJ), Extremely Low Frequency (ELF) radio signals were detected as an emission by the jet itself and they allowed determining the charge transferred upward was negative in most cases (e.g. Su et al., 2003; Soula et al., 2011). Reising et al. (1996) showed that sprite-producing +CG lightning flashes produce large ELF tails following the initial VLF portion, indicating the presence of continuing currents in the discharge. Radio waveforms in ELF range originating in sprite-producing lightning discharges, have been used to estimate the charge removed (Cummer and Inan, 1997; Bell et al., 1998). Cummer et al. (1998) presented the first evidence of electrical currents within the body of sprites by identifying magnetic field waveforms associated with sprites in ELF broad range (from ~3 Hz to ~3 kHz). Stanley et al. (2000) showed clearly that very large day-time sprites were visible

in electric-field-change waveforms. More recent works showed that radio waves could be produced by sprites in ELF (Füllekrug et al., 2001; Rycroft and Odzimek, 2010) and the specific signature could be used for estimating the sprite rate at the Earth surface (Ignaccolo et al., 2006).

During the night of 01-02 September, 2009, very large sprites above a storm located in western Mediterranean Sea close to the French coastline, were recorded by video camera. Several characteristics of the storm and the flashes associated to the sprite events have been analyzed. The second section of the paper describes the data used in this analysis, the third one describes the storm activity along its lifetime and the fourth one presents the conditions of production of the sprite events and their overall characteristics. The fifth section details the chronology of three sequences including very large sprite elements. The sixth section shows some cases of VLF perturbations in possible association with TLEs observed. The seventh section is devoted to a discussion about some aspects of the physics of the sprites.

2. Data and methodology

2.1. Storm characteristics

Data from the French meteorological radar network ARAMIS (from the French "Application Radar à la Météorologie Infra-Synoptique") are used to describe the structure of the storms and they also provide the rainfall pattern. This network consists of 24 Doppler radars (C band and S band) which cover the entire area of mainland France (Parent-du-Châtelet et al., 2003). They have a range of approximately 250 km and systematically produce data for processing plan position indicator (PPI)-type images of the reflectivity factor every 5 minutes with a resolution of 1×1 km^2. Because of the low elevation of the radar beam in conventional mode, these images correspond to the cloud systems at low altitudes. The cloud-top temperatures are provided by the Meteosat satellite from European Organization for the Exploitation of Meteorological Satellites (EUMETSAT) based on radiometer data in the thermal infrared band (IR) at 10.5-12.5 μm. The temperature accuracy is generally better than 1 K which is an irrelevant uncertainty for this study. The parallax error (~15 km for a cloud top at 12 km) is taken into account for the plots which associate the locations of CG flashes with their parent clouds.

2.2. Lightning activity

A lightning detection network, European Cooperation for Lightning Detection (EUCLID), provides data enabling the identification of location, polarity, peak current value, number of strokes, and timing of CG flashes. The network run by Météorage on French territory includes 18 sensors which detect radiation in LF range produced by the return strokes of CG flashes. All sensors use both magnetic direction finding (MDF) and time of arrival (TOA) techniques to determine the location of CG strokes (Cummins et al., 1998). The detection efficiency is ~90% inland and close to the coastline. Consecutive strokes are associated in the same CG flash if they occur within 5 km of the first stroke and within 0.5 s from the previous stroke. Data from a second lightning detection network (LINET) operated by the University of Munich are used to complete the identification of the CG flashes which generate the sprite events. This system uses the MDF and TOA techniques in the Very Low Frequency (VLF)/Low Frequency (LF) range (Betz et al., 2004), and covers the French territory by using a number of sensors distributed over the country. The analysis of the overall CG lightning activity produced by the storm is made from the first system alone.

2.3. Broadband EM radiations

Observations of broadband ELF/VLF activity have been performed with two systems. One is installed in the centre of France (47.27N; 2.63E; ~500 km from the storm location) and has been described in Farges and Blanc (2011). The basic principle is to measure the vertical electric field from lightning and TLE in the vicinity of the source (i.e. within distances lower than 1000 km). This station is equipped with a vertical electric field antenna mounted on a mast, and a computer used for data digitalization and archiving. The antenna used in this study is a dipole antenna designed and manufactured by the French government-funded technological research organization “Commissariat à l’Energie Atomique” (CEA). Its pass-band ranges from less than few hundreds of Hz to 10 MHz. The response inside this band is flat and the antenna factor well known. The performances of the digitalization cards inside the computer are 14-bit resolution, 100 MHz sampling frequency and high memory storage (several tens of milliseconds). Data are GPS stamped. They are acquired when the

signal overtakes a threshold (corresponding to electric field amplitude of 2 V m^{-1}). Another system was located at University of Bath (51.71N; 2.32W; ~1200 km from the storm location). It consists of a wideband digital low-frequency radio receiver described in Füllekrug (2010). The system includes a metal plate insulated from the ground to measure the vertical electric field, a precise GPS clock for timing the data acquisition circuit, and an analogue signal conditioning and data acquisition unit. This instrument has the capability to record electric field strengths in the frequency range from ~4 Hz to ~400 kHz with a sampling frequency of 1 MHz, and an amplitude resolution of ~35 μV m^{-1} and a timing accuracy of ~12 ns.

2.4. ELF signals

The vertical electric and two horizontal magnetic components of the atmospheric electromagnetic field have been monitored simultaneously in a frequency band of 5-30 Hz in the Széchenyi Isván Geophysical Observatory near Nagycenk, Hungary (NCK; 47.62N; 16.72E) at a distance of ~1100 km from the storm. The analogue signals are sampled and digitized at 514.28 Hz for each field component (Sátori et al., 1996; Sátori, 2007). The ELF radiation produced in very intense lightning discharges (mostly CG flashes) occurring all around the globe is detected by this system and the records can be used to estimate the charge moment change (CMC) during the discharge as well as to find out its polarity. The method which is used to process the data from NCK operates in the frequency domain as it is described in Huang et al. (1999). In the calculations, it is assumed that the source current moment decays exponentially in time and that the energy of the detected electromagnetic waves is in the zero order transverse electromagnetic mode. Despite of these seemingly crude simplifications, the method gives back valid CMC estimates especially for individual, intense +CG lightning discharges, the large fraction of which is a single stroke flash (Saba et al., 2010), and for greater source-observer distances (SOD), where the wave energy in propagating modes of higher order than the zero one has already been dissipated. The method has been successfully applied on NCK data in order to characterize the CMCs of sprite producing lightning flashes in previous TLE observation campaigns (Neubert et al., 2005; Yair et al., 2009; Williams et al., 2010). The uncertainty of the deduced CMC values by this method is generally evaluated at ±20% (Williams et al., 2010).

For the sources considered in this study, it must be noted that the SODs are on the border at which the validity of the assumption that only a single wave propagation mode exists is about to fall off. At shorter SODs, having energy in more propagation modes can cause a bias in the deduced CMC estimations. Another consequence of being closer to the source is that events which produce strong ELF radiation saturate the receiving system more likely. This in fact happens for two sprite-producing (P+CG) strokes in this study: events 3 and 6 in Table 1. Other issues which prohibit obtaining valid CMC results with the applied method are low amplitude signals below background noise levels, highly non-exponential current variation in the source (a probable scenario for events 13 and 14 in Table 1) and overlap of the signals from more sources (e.g. for event 4 in Table 1). On the other hand, different sources with exponential-like characteristics occurring close to each other both in space and in time (i.e. quasi-total overlapping) can produce indistinguishable but altogether well processed signals. The deduced CMC value in such cases is the total CMC of all involved source processes. An example for this scenario in this dataset is the case of event 9. Since also the sprites themselves can radiate ELF waves, the deduced CMC can include that in the body of the sprite, too. This is the most probable for intense sprite events appearing shortly after the parent lightning stroke, like those correspond to events 8 and 14 in Table 1. Detection systems of wider passband towards higher frequencies are able to resolve source processes on shorter timescales (Cummer, 2003), as it will be demonstrated also in this paper in the discussed case studies.

2.5. Optical observations

During this specific night of observations, the optical camera system was located at the Pic du Midi (42.93N; 0.14E; 2877 m). It includes one low-light and high-resolution charge-coupled device (CCD) camera (Watec 902H) mounted on a pan-tilt unit remotely controlled by the Internet. It is equipped with a 12 mm f/0.8 lens with a 31° field of view (FOV). The time resolution is 20 ms. The GPS time collected thanks to an antenna is inserted in the images thanks to a video time inserter device from the company PFD Systems (KIWI OSD). Sprites azimuth and elevation are deduced from the video imagery by using the software “Cartes du Ciel” (SkyCharts) as described in van der Velde (2008). This software

allows us overlaying calculated stars over an image, given a certain time, location and part of the sky. The matching of stars with those in the image needs to be done by hand, but works very well if the camera direction and time are known and enough stars are visible. The accuracy of the azimuths for an event depends on the focal length of the lens and resolution of the camera. A sprite is usually much wider than the read-out of azimuth, which varies typically only within 10 arcminutes. The error at 300 km distance is lower than 1 km. Altitude calculations are also based on the measured elevation of the TLE elements in Sky Charts software and on more elaborate calculation to find the altitude above the Earth's surface, taking into account the curvature. The distance to the TLE is considered to be that of the associated +CG flash and according to the uncertainty about the relative position (São Sabbas et al., 2003), the altitude estimation may have a significant error at the distance of the present storm. For example, an error of 10 km for the distance leads to an error of 3.5 km for the top of the sprite. According to the possible displacement of the sprite relative to its parent CG flash (in average 40 km according to São Sabbas et al.), the error on the altitude can reach about 15 km for the top of a large sprite and about 5 km for its bottom.

3. Storm activity

On 1 September 2009, a low-pressure area located northwest of Ireland and a trough of pressure west of Portugal drove a north-eastward flow over northern Spain and France (Fig. 1). With warm air at lower layer in these regions, the instability favoured the storm development. Large CAPE values are reported (1923 J kg^{-1} from sounding in Barcelona on Sept 1 at 1200 UT). During the evening, a storm developed in northern Spain and moved eastward over Gulf of Lion during the night, as illustrated in Fig. 2 with the cloud top temperature issued from infrared radiometer (10.5/12.5 μm) of the Meteosat Second Generation (MSG) at 1825 UT (a), 0110 UT (b) and at 0240 UT (c) (times of the scan over the storm area). The CG flashes detected over 10 minutes surrounding the time of scan of the storm are also displayed in Fig. 2. The CG flashes concentrate within the regions with the coldest cloud top temperature (~-70 °C). The location of Pic du Midi (42.93N and 0.14E) from where the TLEs were observed during the night is indicated by a white triangle. Fig. 3 displays the CG lightning flash density calculated within 5×5 km^2 areas for the whole storm

lifetime. Most CG flashes were produced when the storm was located over sea in the Gulf of Lion, where the density reaches close to 2 km^{-2}, a very large value for the CG flashes produced by only one storm. The locations of the 15 P+CG flashes (squares in Fig. 3) are all over sea and for the majority out of the area of high CG flash density.

Fig. 4a displays the time series of the area of the cloud for several intervals of its top temperature (histograms) and that of the minimum value of the cloud top temperature (line). The storm development clearly exhibits two periods with a maximum of the total area (around 2100 and 0300 UT) largely preceded by a minimum of the cloud top temperature (around 1800 and 0030 UT). The value of the temperature is about -71 °C for both minima observed. The size of the thundercloud the temperature of which is colder than -35 °C reaches between 90,000 and 100,000 km^2 for the first maximum, and about 70,000 km^2 for the second one. Fig. 4b displays the rates of CG lightning flashes for both polarities (histograms) and the +CG proportion (lines). The maximum values of CG flash rate (around 1830 UT and 0115 UT) are relatively well synchronized with the minima of the cloud top temperature and precede the cloud extension. This coincidence can be explained by the presence of strong updrafts which are favorable for both the cloud electrification processes and its vertical development. The second period of CG lightning activity is much stronger with a maximum rate close to 45 min^{-1} (~18 min^{-1} for the first period), although the size of the cloud is about the same. The large and fast increase of the CG flash rate around 0100 UT corresponds to the minimum of the cloud top temperature. The CG flashes are produced when the storm is over sea and leads to the largest densities as shown in Fig. 3. After the CG flash rate reaches the maximum at 0110 UT, it decreases rapidly for both polarities and some CG flashes are produced until 0310 UT. The +CG flash proportion varies substantially during the whole storm lifetime. Its minimum and maximum values before ~0310 UT are 10.4% at 0000 UT and 68.3% at 2145 UT, respectively. This proportion is therefore relatively high, especially when the CG flash rate exhibits low values and during the TLE observation period. Fig. 4c displays the average peak current for both CG flash polarities. A significant increase of the average peak current of the +CG flashes is observed during the sprite observation period.

4. Conditions of production and characteristics of sprites

The period during which sprites were observed is indicated in Fig. 4 with an arrow

(0209-0307 UT). It is short in comparison to the whole storm lifetime with about 8 hours in night conditions. However, the sky above the observation site was clear enough for observation in the direction of the storm only after 0000 UT. As indicated in Fig. 2b the visibility was good at the site when the CG flash rate was high around 0100 UT and the camera pointed already in the storm direction. It is not possible to know if TLEs were produced before 0000 UT because the sky was partly cloudy above the camera.

According to Fig. 4, during the observation period (0209 - 0307 UT), the CG flash rate is low, the cloud area increases (especially that with a top temperature between -60 °C and -45 °C), and the average peak current for positive CG flashes is large. The characteristics of the sprite events and their P+CG strokes are summarized in Table 1. Nine videos with TLEs have been recorded including 17 sprite events, 15 of which are associated with a +CG stroke and 2 are apparently associated with IC activity, detected a few tens of ms before by LINET and/or ELF/VLF. We cannot exclude CG flashes produced before these two events were missed by the detection system. Several sprite events are distinctly considered within a same video when they are separated by at least one frame without any sprite luminosity and/or when a potential CG parent flash is detected (or visible in the video imagery) between them. For the present cases, we could easily distinguish four events in one video, three events in one video, two events in three videos, and one event in four videos. The time indicated for the sprite event is that of the beginning of the first frame (video frames are separated by 20 ms). The peak current of the P+CG strokes ranges between 11.6 and 216.4 kA. However, the +CG stroke with a peak current of 11.6 kA is detected 20 ms after the beginning of the first frame including the sprite, which is exactly the largest value physically possible. The possibility that a parent stroke was missed by the detection systems is not excluded in this case also. A majority of sprite events are carrot-type and most of them have several elements. Three sprites of carrot-type are associated with a halo. Fig. 5 shows some examples of sprites and halos with the vertical scale superimposed. This scale is calculated and valid at the distance of the sprite to the camera which is estimated as that of the P+CG stroke and ranges from 280 km to 390 km. Some sprites have very large vertical and horizontal dimensions, especially those at 2h 33min 16s and 3h 07min 43s (altitude from ~30±5 km to close to 100±15 km, ~80±2 km horizontally). The carrot-type elements of these large sprites are becoming smaller and

smaller towards the edges of the group and seem to converge to a point below the central elements. Their tops produce a diffuse light with some bright branches superimposed which can exceed the altitude of 90±15 km). The halos appear between 65 and 85±10 km of altitude and they are associated with carrot sprites centered below them. The peak current (and CMC when it is available) of the P+CG strokes of these sprite events are 153 kA, 70 kA (1648±20% C km), 20 kA, 142 kA, 216 kA (1678±20% C km), and 86 kA (2088±20% C km), from left to right and from top to bottom in Fig. 5. The peak current has very much more variable values.

Fig. 6 displays the time series of the CG peak current for the storm by distinguishing -CG flashes, +CG flashes and P+CG strokes. During the lifetime of the storm, the -CG flashes exhibit peak current of larger and larger values but they do not produce any visible TLE when the conditions of observation were good. The +CG flashes can exhibit large values (>100 kA) during the whole storm but they produce visible TLEs for a short period after 0200 UT and not around 0100 UT for example. During the period of TLE observation all +CG strokes with a large peak current (>60 kA) have triggered a TLE.

In order to have an idea of the characteristics of the cloud (convective or stratiform) in the region of the CG flashes, the precipitation rates estimated from radar reflectivity have been averaged within circles of 5 km radius around every CG flash produced by the thunderstorm (van der Velde, 2008). This estimation has been applied in an area from 0.9° to 6° in longitude and from 41° to 44.5° in latitude in order to eliminate the CG flashes which stand out of the storm considered in the study. CG flashes observed from 2200 UT on 1 September to 0400 UT on 2 September have been selected. The number of included radar pixels in each circle may vary somewhat according to the location of a CG flash relative to the radar pixel grid. The grid is composed of squares of approximately 1 km² area. Radar reflectivity Z, typically expressed in dBZ, is related to a factor Z_0 by a logarithm law: $Z = 10 \log Z_0$. Z_0 (in $mm^6\ m^{-3}$) is proportional to the density of particles n and their diameter D ($Z_0 \propto n D^6$) in the volume scanned by the radar beam. For non-critical use as in this study, reflectivity Z_0 can be conveniently converted to the rainfall rate R by the commonly used empirical Z-R relationship stemming from the Marshall and Palmer (1948) drop size distribution: $Z_0 = 200 R^{1.6}$ (Z_0 in $mm\ m^{-3}$ and R in $mm\ h^{-1}$).

Fig. 7a displays the distribution of the average precipitation rate within 5 km distance

around the +CG and -CG flashes versus their peak current. The strongest discharges are mostly produced in weak to moderate precipitation (<30 mm h^{-1}), but weak precipitation produces many weak discharges as well. The peak currents progressively increase in absolute value with decreasing average precipitation. However both sides of the distribution for -CG flashes and for +CG flashes are not really symmetrical. As a matter of fact, it is wider for -CG flashes especially for precipitation rates larger than 20 mm h^{-1}, i.e. the negative peak current can be larger in absolute value at a given value of the rain rate. On the contrary, at very low values of the rain rate (<10 mm h^{-1}) the positive peak current have larger values. The mean precipitation rate for +CG flashes is 31.8 mm h^{-1} with a mean positive peak current of 15.78 kA, while that for -CG flashes is 36.5 mm h^{-1} with a mean negative peak current of -24.43 kA. The P+CG strokes (triangles in Fig. 7a and b) are produced in regions with a precipitation rate lower than 11 mm h^{-1} and approximately equal to 5 mm h^{-1} in average. More than 60% of the P+CG strokes are located in a region where the precipitation rate is lower than 5 mm h^{-1}. The precipitation rate also evolves with time: between 2200 and 0000 UT, most of the CG flashes are associated with a rate lower than 35 mm h^{-1} and the average rate is quite weak (12 mm h^{-1}). Between 0000 and 0200 UT, the precipitation rate increases to an average value of 47 mm h^{-1} with some values over 100 mm h^{-1}. The average rate decreases during the TLE observation before becoming extremely low between 0300 and 0400 UT at a value of 3.2 mm h^{-1}.

The average precipitation rate has been also calculated within 10 km distance around the +CG and -CG flashes. The difference between the precipitation rates of the 5- and 10-kilometer circles for individual CG flashes can be an indication of the uniformity of precipitation (Fig. 7b). The CG flashes of both polarities tend to occur close to a core of precipitation since the majority of CG-associated differences of precipitation rate between 5 and 10 km are positive. All peak currents higher than 100 kA occur in regions where the precipitation is rather uniform with a difference of rate lower than 20 mm h^{-1}. The temporal evolution is the same as before: the difference in precipitation rate is lower than 20 mm h^{-1} for all CG flashes between 2200 and 0000 UT, increases after 0000 UT and reaches its maximum between 0100 and 0200 UT with values higher than 60 mm h^{-1} before quickly decreasing. The P+CG strokes occur in regions with a strong precipitation uniformity since difference in precipitation rate is, in absolute value, lower than 5 mm h^{-1} for all of them and lower than 2

mm h^{-1} for more than 85% of them.

5. Analysis of sprite sequences

5.1. Sequence at 02h 33min 16s

Fig. 8a displays four successive video frames (80 ms) starting at 02h 33min 16.706s UT including three sprite events (events 2, 3 and 4 in Table 1). Within these frames, $d_{1\text{-}4}$ indicates the location of four lines of sight which are reported in Fig. 8d. Fig. 8b displays the chronology of the four video frames and the strokes associated with the sprite events thanks to their peak current, two P+CG strokes and one IC discharge detected by Linet. Fig. 8c shows the ELF/VLF/LF electric field variation from 10 ms before the second P+CG stroke to 15 ms after. Fig. 8d displays the stroke locations and the four sprite lines of sight superimposed to the radar reflectivity field in F_2 at 0235 UT.

The sequence starts at t=16.670 s with IC lightning activity according to Linet detection. Following this IC discharge, a sprite event is visible in the video imagery (frame at t=16.686-16.706 s, not shown). Frame 1 in Fig. 8a (t=16.706-16.726 s) shows this sprite is a group of column-type elements. A P+CG stroke at t=16.739 s with a peak current of 33 kA is assumed to have triggered the carrot-type sprite visible in direction d_2 in frame 2 (t=16.726-16.746 s). A second and strong P+CG stroke with a peak current of 153 kA immediately follows at t=16.750 s and triggers the bright and large group of sprites shown in frame 3 (t=16.746-16.766 s) of Fig. 8a, between d_1 and d_3. The central elements of this group are particularly extended downward and as a consequence, a connection between the sprites and the upper part of the thundercloud could be possible. As a matter of fact, the lower part of the sprites remains bright above the cloud and corresponds with the direction d_4 in frame 4 (t=16.766-16.786 s) of Fig. 8a. This phenomenon could be identified as a “troll” (Heavner, 2000).

The electric field variation in ELF range (lower graph of Fig. 8c) exhibits a first jump synchronized with the second P+CG stroke and a second jump, 2 ms later, in the same polarity. The first jump corresponds to a positive charge moving downward and the second is assumed to correspond to negative charge moving upward. VLF (middle graph) and LF (upper graph) electric field variations exhibit a quite strong and short peak at t=0 ms (t=16.750 s in Fig. 8b),

as a signature of the P+CG stroke.

Fig. 8d shows that both P+CG strokes occur in the stratiform part of the thundercloud, where reflectivity is generally lower than 35 dBZ (~5 mm h^{-1}). This Figure allows identifying the trailing-stratiform structure of the MCS with the convective line at the northeastern part i.e. at the front of the system according its moving to the northeast. The IC discharge corresponds exactly with the location of the second P+CG stroke (noted (2) in the graph). The location of the first P+CG stroke (noted (1) in the graph) is shifted from d_2 which corresponds to the sprite in frame 2. On the contrary, the location of the second P+CG stroke corresponds to d_4, common direction to the centre of the bright event and to the remaining "troll" in frame 4. The shift observed for the first P+CG stroke could be explained by the fact that the detection network records CG strokes which can be located far from the effectively discharged part of the cloud. The first P+CG stroke is clearly closer to the convective line compared to the second one.

5.2. Sequence at 2h 41min 17s

Fig. 9a displays three video frames including two sprite events (events 7 and 8 in Table 1). The first video frame starts at 02h 41min 17.128s UT. $d_{1\text{-}3}$ indicates the location of three lines of sight which are reported in Fig. 9d. Fig. 9b displays the chronology of the three video frames and the strokes associated with the sprite events thanks to their peak current, two P+CG strokes and one -CG stroke. The CMC of the second P+CG stroke has been calculated and is also reported in Fig. 9b. Lower graph of Fig. 9c shows the spectrum of the electric field radiated in broad band (ELF to LF) from 10 ms before the second P+CG stroke to 15 ms after, while the upper graph and the middle graph display the same parameter in VLF and ELF ranges, respectively. Fig. 9d displays the CG stroke locations and the three sprite lines of sight superimposed to the radar reflectivity field at 0240 UT.

The sequence starts with a P+CG stroke with a low peak current of 18 kA detected at t=17.080 s. This P+CG stroke triggers the column sprites centred in d_1 at t=17.128-17.148 s as seen in frame 1 of Fig. 9a. These column sprites are not very bright and remain visible within three video frames, with possible new elements as observed in frame 2 (t=17.148-17.168 s). A -CG stroke with a weak peak current of -8 kA occurs at t=17.156 s. A P+CG stroke with a

peak current of 70 kA at t=17.202 s triggers the carrot sprites recorded in frame 3 (t=17.188-17.208 s). This group of very bright carrot sprites spread between d_2 and d_3. A CMC of 1648±20% C km is associated to this second P+CG stroke. The largest electric field variations generated by the second P+CG stroke are observed at frequencies lower than 100 kHz and for less than 1 millisecond as seen in lower graph of Fig. 9c. Nevertheless, according to middle graph of Fig. 9c, the ELF perturbation exhibits two peaks: one which corresponds with the P+CG stroke and another ~4 ms after, which may correspond to the sprite discharge. Both P+CG strokes are located in the stratiform part of the thundercloud where the radar reflectivity is lower than 30 dBZ (~3 mm h^{-1}) as seen in Fig. 9d. The first P+CG stroke location is shifted from the direction d_1 indicating the centre of the column sprites displayed in frame 1. On the contrary, the second one seems to be located just beneath the lower part of the carrot sprites displayed in frame 3 and delimited by direction d_2 and d_3. The -CG stroke is located very close to the first P+CG stroke and in the same direction of the brightest sprite element in frame 2, i.e. slightly shifted to the north from d_1.

5.3. Sequence at 03h 07min 43s

Fig. 10a displays four video frames including three sprite events (events 15, 16 and 17 in Table 1). The first video frame starts at 03h 07min 43.577s UT. $d_{1\text{-}4}$ indicates the location of four lines of sight which are reported in Fig. 10d. Fig. 10b displays the chronology of the four video frames and the strokes associated with the sprite events thanks to their peak current, two P+CG strokes and one IC discharge detected by Linet. Fig. 10c shows the ELF/VLF/LF electric field variation from 10 ms before both P+CG strokes to 15 ms after. Fig. 10d displays the flash locations and the four lines of sight of sprite ($d_{1\text{-}4}$) superimposed to the radar reflectivity field at 0310 UT.

The sequence starts at t=43.586 s with the first and strong P+CG stroke, with a peak current of 216 kA and a CMC of 1678±20% C km. Its duration is 291 ms until the end of the frame 4 shown in Fig. 10a (43.877 s). We can distinguish four distinct periods during this sequence: (1) between 43.586 s and 43.637 s, sprite elements with halo, carrot, columns are associated with the +CG flash at 43.586 s and visible for example in frame 1 (t=0.577-0.597 s) of Fig. 10a. The columns are visible on left and right edges of the halo. The P+CG stroke is

well aligned in the direction d_1. (2) No sprite luminosity is visible between 43.637 s and 43.717 s (80 ms) and an IC flash is then detected by Linet at t=0.703 s. (3) Continuous sprite (small columns) and flash luminosity can be seen in the two following frames between 43.717 s and 43.757 s (not shown). In frame 2 of Fig. 10a (t=43.757-43.777 s) a luminous carrot sprite and a stronger flash luminosity occur. No new CG stroke is detected before this carrot sprite but we can suppose one could be missed by the detection system. Sprite elements remain visible between 43.777 s and 43.837 s (60 ms) while flash luminosity is also visible. (4) Between 43.837 s and 43.857 s large carrots are produced (frame 3 of Fig. 10a) and probably associated with the +CG stroke detected at 43.840 s. This second P+CG stroke exhibits a peak current of 85 kA and a CMC of 2090±20% C km. This group of very bright sprite elements spread between d_3 and d_4. Some of these elements are again particularly developed downward and a connection with the top of the cloud might be assumed according to the luminous channel visible in frame 4 (t=0.857-0.877 s), near the top of the cloud in direction d_2.

The ELF signature of the first P+CG stroke is displayed in lower graph of the left side of Fig. 10c and exhibits one peak corresponding to the stroke detection. On the other hand, the ELF signature associated with the second P+CG stroke in the lower graph on the right side of Fig. 10c exhibits two peaks: one corresponding to positive charges carried downwards by the stroke, another about 4 ms after corresponding to negative charge moving upward. This second peak is not visible at higher frequencies unlike to the P+CG stroke, which confirms it cannot be associated with a return stroke. Both P+CG strokes and IC detection are superimposed to the radar reflectivity in Fig. 10d (IC corresponds exactly with the location of the first P+CG stroke noted (1) in the graph). All of them are located in areas where radar reflectivity is lower than 35 dBZ (approximately 5 mm h^{-1}) in the stratiform region of the thundercloud. The line of sight d_1, for the first carrot sprite with halo, matches exactly with the first P+CG stroke noted (1). On the contrary, the carrot sprite of frame 2 aligned in direction d_2, is displaced from the lightning activity detected before in direction d_1. On the contrary, the matching between the lower part of the group of sprite on frame 4 (d_2) and the triggering P+CG stroke (noted (2) in the graph) is very slightly shifted. In this case too, the second P+CG stroke is back in the stratiform region.

6. VLF signals perturbation in association with the sprite events

The connection between the TLEs and the VLF signal perturbations has been previously reported from observations during the Eurosprite campaigns (Haldoupis et al., 2004, 2010; NaitAmor et al., 2010). In these studies, the TLEs were found to be associated with early signals perturbations when the Great Circle Path (GCP) of the electromagnetic (EM) wave passed near the TLE region. The term early refers to the fact that the perturbation occurs nearly in coincidence (within 20 ms) of the lightning stroke (Inan and Rodriguez, 1993). Within early VLF events, early/fast events are characterized by a rapid onset duration (<20ms), whereas early/slow events are characterized with an onset duration of 100-1000 ms. Early VLF events are followed by a slow recovery (between 10 to 100 s or more, Inan et al., 1996). The perturbation parameters (amplitude and duration) were function of the distances between the TLE and the transmitters and between the TLE and the receivers, and the scattering angle of the EM by the TLE body (NaitAmor et al., 2010). The data recorded at Algiers showed that sprites observed at Pic du Midi were the sources of early signals perturbations in the DHO-Algiers and NAA-Algiers paths.

Sprite locations and transmitter-receiver paths considered in this study are plotted in Fig. 11a. For the event at 2h 33min 16s (Fig. 8) the perturbation is visible in both paths to Algiers according to the graphs in Fig. 11b. The DHO path crosses the sprite region but the NAA path is completely far from it. The amplitude and the duration of the perturbation for the DHO signal are low which could be due to the modal structure of the EM wave at the sprite location. For the NAA signal, the perturbation is due to the wide scattering angle of the EM wave by the sprite. The existence of the perturbation in the NAA path is a clear evidence of a large number of particles produced in the disturbed region. For the event at 2h 41min 17s, the DHO signal shows a perturbation starting at 02h 37min 28s which is associated with another sprite event (Fig. 11b). So the signal is a continuity of the perturbation which lasts more than 6 minutes. For the NAA path only the lightning emission in the VLF band (or sferic) has been recorded. Concerning the case of the sprite event detected at 3h 07min 43s, the perturbations are also recorded in both paths as indicated in Fig. 11b. The perturbation parameters are small in the case of the DHO signal and very large (0.5 dB in amplitude and 80 s in duration) in the

case of the NAA signal. The perturbation recorded at the NAA path is also due to the wide scattering angle of the EM wave by the sprite body like in the first case.

7. Discussion and conclusion

During a TLE-producing sequence of a long-lifetime storm, 17 TLE events were observed from a unique station using a video camera. These events (17 sprites, 3 of which with halo) are divided into nine short videos (between 1.5 and 2 s). There are five videos with multiple TLE events (separated with at least one video frame and triggered by a new P+CG stroke), one with four TLE events, one with three and three with two. Both types of sprite, column and carrot, are observed and some events are groups of very large carrots. The columns generally occur either alone within the event or at the beginning of the event preceding large carrots. However, some column elements are observed to evolve into carrot elements from a frame to the next. As shown in Montanyà et al. (2010) and in Stenbaek et al. (2010) thanks to fast camera observations, the carrot elements are due to upward streamers which develop after the columns formed by downward streamers. Upward streamers are generally observed when the downward streamers are initiated at lower altitude. Our video observations do not allow identifying such a detailed evolution directly, but the estimated streamer initiation time within the sequence of the video frames confirms the proposed temporal evolution.

All very large carrot sprites are preceded by other sprite events within a few tens of milliseconds. Thanks to an enhancement of ionization in the mesosphere, these first sprites could create better conditions for sprite initiation when a new +CG stroke occurs rapidly, according to the mechanism proposed by Pasko et al. (1997) for sprite generation. As a matter of fact, the streamer electric breakdown has been used to explain the observed highly structured regions of sprites (e.g. Pasko et al. 1998a). It is well described in Pasko et al. (2000) that, in order to initiate a streamer, an electric field exceeding the conventional breakdown threshold (E_k) is needed. Once it is initiated, it can propagate while the electric field is more intense than the minimum fields required for streamer propagation for each polarity (E_{cr}^{+} , E_{cr}^{-}). In a basic approach, these critical fields E_{cr}^{+} and E_{cr}^{-} defines the extension of the altitudes that a sprite may reach. The altitudes where the electric field is higher (for each

polarity) are defined, among other factors, by the amount of charge lowered by the associated lightning flash and the altitude from which this charge is removed. However, some other effects must be considered such as the duration of the charge removal and additional charge removal by multiple lightning activities. In the cases presented here we cannot reject any of the proposed causes of the large size of the observed sprites. In all three cases multiple lightning activities have been detected. This would be favorable for high amount of charge removal and indicates long duration of the events. Moreover, high peak currents with very high CMC are estimated. These CMCs would suggest high charge removal and/or high charge reservoirs. All these effects would lead to decrease the altitudes of the critical propagation fields E_{cr}^{+} and E_{cr}^{-} and would allow the streamer propagating at lower altitudes. On the other hand, the enhancement of the transient electric field with multiple +CG lightning strokes would let to increase the volume of the conditions necessary to initiate and to propagate the streamers. These would explain the unusual size of the observed sprites.

Some halos are clearly visible and always associated with a sprite (column or carrot). In this case, the halo occur around 70-80 km of altitude as previously indicated by Wescott et al. (2001). The present large sprite events which can be considered as part of the largest ones among the works previously published, show the maximum altitude of sprite can reach and slightly exceed 90 km as previously described by Sentman et al. (1995). On the other hand, these events show also the sprite tendrils can reach below 40 km and even around 30 km, which is much more rarely observed but however suggested by Lyons (2006). The question about a physical connection of the tendrils with the top of the parent storm is open and the present observations of small and fuzzy channels remaining after the most developed sprites can suggest this kind of link as observed in the troll events (Heavner, 2000). On the other hand, the signatures of these sprite events in ELF range exhibit a second peak after that produced by the P+CG stroke. This second peak occurs within about 5 ms after the P+CG stroke and in the timed video frames which display the large sprite. This signature is observed for the three largest sprite cases which are also the brightest sprites. The time delay of ~5 ms with respect to the parent lightning discharges is similar to the time delays reported by Cummer et al. (1998). Cummer et al. found the amplitude of the source current moment peak

was proportional to the brightness of the sprite. Pasko et al. (1998b) explains the mechanism of ELF radiation by sprite with a delay of a few milliseconds. The present bright sprite events confirm that large currents can flow in the body of sprites.

The average peak current of the 15 P+CG strokes identified is 83 kA while that of the 12 P+CG strokes corresponding with the sprites alone is 67 kA. This latter value is very consistent with that given in Soula et al. (2010) which was 63 kA and also with values given in previous works which were around 60 kA (e.g. Sao Sabbas et al., 2003; Pinto et al., 2004; Soula et al., 2009). As in Soula et al. (2010) the peak current for the P+CG strokes producing halos is much higher since it ranges from 89 to 216 kA. However, not all P+CG strokes with a large peak current produce a visible halo.

All P+CG strokes are located in the stratiform region of the trailing-stratiform MCS, characterized with a rain rate lower than 10 mm h^{-1} which is also the common observation in many sprite-producing storm studies (e.g. Lyons, 1996; Soula et al., 2009). In the five cases of multiple TLE events, the first P+CG stroke is closer to the convective line and the following P+CG strokes are displaced towards the stratiform region as indicated by van der Velde et al. (2010). By using VHF detection in northern Spain, van der Velde et al. showed that the convective-to-stratiform propagation of long intracloud channels was associated to such multiple P+CG strokes, confirming previous observations in other regions of the world (e.g. Lyons et al., 2003; Lang et al., 2004). The sequence of the TLE produced by the storm and observed by the camera is characterized by a very low CG flash rate preceded by a very active period in terms of its CG lightning activity.

The observations confirm that the TLEs are mostly in association with VLF signals perturbations due to conductivity changes of the ionospheric D-region. Despite that the GCP paths of the GQD, NRK and HWU are closer to the location of the events, only the CG flash signatures were recorded. This keeps the question on the association between TLEs and early VLF signals perturbations open.

Acknowledgments

The authors thank the helpful comments of two anonymous reviewers that have led to

improvements of the paper. They also thank Jean-Pierre Olry from SATMOS for providing Meteosat observations. They would like to thank Météorage, for providing the data on the CG lightning flashes and MétéoFrance, the French weather service, for providing the data from the radar network. They thank Professor Betz from the University of Munich for providing data of lightning location from LINET network. The contribution of SS to this work was supported by the Centre National d'Etudes Spatiales (CNES). The contribution of OvdV and JM was possible thanks to grant AYA2009-14027-C05-05 of the Spanish Ministry of Science and Innovation. Contribution of JB was supported by the Hungarian Scientific Research Fund (OTKA: K72474). The work of MF is supported by the Natural Environment Research Council under grant no. NE/H024921/1.

References

Bell, T.F., Reising, S.C. Inan, U.S., 1998. Intense continuing currents following positive cloud-to-ground lightning associated with red sprites. Geophys. Res. Lett. 25, 1285-1288.

Boccippio, D.J., Williams, E.R. Heckman, S.J. Lyons, W.A. Baker, I.T. Boldi R., 1995. Sprites, ELF transients, and positive ground strokes. Science 269, 1088.

Chen, A.B., et al., 2008. Global distributions and occurrence rates of transient luminous events. J. Geophys. Res. 113, A08306. doi:10.1029/2008JA013101.

Cummer, S.A., 2003. Current moment in sprite-producing lightning. J. Atmos. Sol.-Terr. Phys. 65, 499-508.

Cummer, S.A., Inan, U.S., 1997. Measurement of charge transfer in sprite-producing lightning using ELF radio atmospherics. Geophys. Res. Lett. 24, 1731-1734.

Cummer, S.A., Stanley, M., 1999. Submillisecond resolution lightning currents and sprite development: Observations and implications. Geophys. Res. Lett., 26, 3205-3208.

Cummer, S.A., Inan, U.S., Bell, T.F., Barrington-Leigh, C.P., 1998. ELF radiation produced by electrical currents in sprites. Geophys. Res. Lett., 25, 1281-1284.

Cummins, K.L., Murphy, M.J., Bardo, E.A. Hiscox, W.L., Pyle, R.B., Pifer, A.E., 1998. NLDN'95, a combined TOA/MDF technology upgrade of the US National Lightning Detection Network. J. Geophys. Res. 103, 9035–9044.

Farges, T., Blanc, E., 2011. Lightning and TLE electric fields and their impact on the

ionosphere. C. R. Physique 12, 171-179.

Füllekrug, M., 2010. Wideband digital low-frequency radio receiver. Meas. Sci. Technol. 21, 015901. doi:10.1088/0957-0233/21/1/015901.

Füllekrug, M., Moudry, D.R., Dawes, G., Sentman D.D., 2001. Mesospheric sprite current triangulation. J. Geophys. Res., 106, 20,189-20,194.

Hayakawa, M., Nakamura, T., Hobara, Y., Williams, E.R., 2004. Observation of sprites over the Sea of Japan and conditions for lightning-induced sprites in winter. J. Geophys. Res., 109, A01312. doi:10.1029/2003JA009905.

Haldoupis, C., Neubert, T., Inan, U.S., Mika, A., Allin, T.H. Marshall R.A., 2004. Subionospheric early VLF signal perturbations observed in one-to-one association with sprites. J. Geophys. Res., 109, A10303. doi:10.1029/2004JA010651.

Haldoupis, C., Amvrosiadi, N., Cotts, B.R.T., van der Velde, O.A., Chanrion, O., Neubert, T., 2010. More evidence for a one-to-one correlation between Sprites and Early VLF perturbations. J. Geophys. Res., 115, A07304. doi:10.1029/2009JA015165.

Heavner, M., 2000. PhD dissertation, University of Alaska Fairbanks, USA.

Huang, E., Williams, E.R., Boldi, R., Heckman, S., Lyons, W., Taylor, M., Nelson, T., Wong C., 1999. Criteria for sprites and elves based on Schumann resonance observations. J. Geophys. Res., 104, 16,943–16,964.

Ignaccolo, M., Farges, T., Mika, A., Allin, T.H., Chanrion, O., Blanc, E., Neubert, T., Fraser-Smith, A.C., Füllekrug M., 2006. The planetary rate of sprite events. Geophys. Res. Lett., 33, L11808. dOI: 10.1029/2005GL025502.

Inan, U.S., Rodriguez, J.V., 1993. VLF signatures of lightning-induced heating and ionisation of the nighttime D region. Geophys. Res. Lett., 20, 2355-2358.

Inan, U.S., Slingeland, A., Pasko V.P., 1996. VLF and LF signatures of mesospheric/Lower ionospheric response to lightning discharges. J. Geophys. Res., 101, 5219-5238.

Lang, T.J., Rutledge, S.A., Wiens, K.C., 2004. Origins of positive cloud-to-ground lightning flashes in the stratiform region of a mesoscale convective system. Geophys. Res. Lett., 31, L10105. doi:10.1029/2004GL019823.

Lyons, W.A., 1996. Sprite observations above the U.S. High Plains in relation to their parent thunderstorm systems. J. Geophys. Res., 101, 29,641–29,652.

Lyons, W.A., Nelson, T.E., Williams, E.R., Cummer, S.A., Stanley M.A., 2003. Characteristics of sprite-producing positive cloud-to-ground lightning during the 19 July 2000 STEPS mesoscale convective systems. Mon. Weather Rev., 131, 2417-2427.

Marshall, J.S., Palmer, W.M., 1948. The distribution of raindrops with size. J. Meteorol. 5, 165–166.

Montanyà, J., van der Velde, O., Romero, D., March, V., Solà, G., Pineda, N., Arrayas, M., Trueba, J.L., Reglero, V., Soula, S., 2010. High-Speed Intensified Video Recordings of Sprites and Elves over the Western Mediterranean Sea during Winter Thunderstorms. J. Geophys. Res., 115, A00E18, doi:10.1029/2009JA014508.

NaitAmor, S., AlAbdoadaim, M.A., Cohen, M.B., Cotts, B.R.T., Soula, S., Chanrion, O., Neubert, T., Abdelatif T., 2010. VLF observations of ionospheric disturbances in association with TLEs from the EuroSprite 2007 campaign. J. Geophys. Res., 115, A00E47. doi:10.1029/2009JA015026.

Neubert T., Allin, T.H., Blanc, E., Farges, T., Haldoupis, C., Mika, A., Soula, S., Knutsson, L., van der Velde, O., Marshall, R.A., Inan, U.S., Sátori, G., Bór, J., Hughes, A., Collier, A., Laursen, S., Rasmussen I.L., 2005. Co-ordinated observations of transient luminous events during the EuroSprite2003 campaign. J. Atmos. Sol.-Terr. Phys., 67, 807-820.

Neubert, T., et al., 2008. Recent results from studies of electric discharges in the mesosphere. Surv. Geophys., 29, doi:10.1007/s10712-008-9043-1.

Parent du Châtelet, J., Guimera, M., Tabary P., 2003. The PANTHERE Project of Meteo-France: Extension and upgrade of the French radar network. 31st Int. Conf. on Radar Meteorology, Am. Meteorol. Soc., Seattle, Wash.

Pasko, V.P., Inan, U.S., Bell, T.F., Taranenko Y.N., 1997. Sprites produced by quasi-electrostatic heating and ionization in the lower ionosphere. J. Geophys. Res., 102, 4529–4562.

Pasko, V.P., Inan, U.S., Bell T.F., 1998a. Spatial structure of sprites. Geophys. Res. Lett., 25, 2123-2126.

Pasko, V.P., Inan, U.S., Bell, T.F., Reising S.C., 1998b. Mechanism of ELF radiation from sprites. Geophys. Res. Lett., 25. doi:10.1029/98GL02631.

Pasko, V.P., Inan, U.S., Bell T.F., 2000. Fractal structure of sprites. Geophys. Res. Lett., 27,

497-500.

Pinto, O.Jr., Saba, M.M.F., Pinto, I.R.C.A., Tavares, F.S.S., Naccarato, K.P., Solorzano, N.N., Taylor, M.J., Pautet, P.D., Holzworth, R.H., 2004. Thunderstorm and lightning characteristics associated with sprites in Brazil. Geophys. Res. Lett., 31, L13103. doi:10.1029/2004GL020264.

Reising, S.C., Inan, U.S., Bell, T.F., Lyons, W.A., 1996. Evidence for continuing currents in sprite-producing lightning flashes. Geophys. Res. Lett., 23, 3639-3642.

Rycroft, M.J., Odzimek, A., 2010. Effects of lightning and sprites on the ionospheric potential, and threshold effects on sprite initiation, obtained using an analog model of the global atmospheric electric circuit. J. Geophys. Res., 115, A00E37. doi:10/1029/2009JA014758.

Saba, M.M.F., Schulz, W., Warner, T.A., Campos, L.Z.S., Schumann, C., Krider, E.P., Cummins, K.L., Orville, R.E., 2010. High-speed video observations of positive lightning flashes to ground. J. Geophys. Res., 115, D24201. doi:10.1029/2010JD014330.

São Sabbas, F.T.S., Sentman, D.D., Wescott, E.M., Pinto, J O., Mendes, J.O., Taylor, M.J., 2003. Statistical analysis of space-time relationships between sprites and lightning. J. Atmos. Sol.-Terr. Phys., 65, 525-536.

Sátori, G., 2007. Schumann resonance observations. Geophysical Observatory Reports of the Geodetic and Geophysical Research Institute of the Hungarian Academy of Sciences, edited by V. Wesztergom, pp. 75-80, Nagycenk Geophys. Obs., Nagycenk, Hungary.

Sátori, G., Szendrői J., Verő, J., 1996. Monitoring Schumann resonances 1. Methodology. J. Atm. Sol.-Terr. Phys., 58, 1475-1481.

Sentman, D.D., Wescott, E.M., Osborne, D.L., Hampton, D.L., Heavner, M.J., 1995. Preliminary results from the Sprites 94 aircraft campaign: 1. Red sprites. Geophys. Res. Lett., 22, 1205-1208.

Soula, S., van der Velde, O., Montanyà, J., Neubert, T., Chanrion, O., Ganot, M., 2009. Analysis of thunderstorm and lightning activity associated with sprites observed during the EuroSprite campaigns: two case studies. Atmos. Res., 91. doi:10.1016/j.atmosres.2008.06.017.

Soula, S., van der Velde, O., Palmieri, J., Montanyà, J., Chanrion, O., Neubert , T., Gangneron, F., Meyerfeld, Y., Lefeuvre, F., Lointier, G., 2010. Characteristics and conditions of

production of transient luminous events observed over a maritime storm. J. Geophys. Res., 115, D16118. doi:10.1029/2009JD012066.

Soula, S., van der Velde, O., Montanyà, J., Huet, P., Barthe, C., Bór, J., 2011. Gigantic jets produced by an isolated tropical thunderstorm near Réunion Island. J. Geophys. Res., 116, D19103. doi:10.1029/2010JD015581.

Stanley, M., Brook, M., Krehbiel, P., Cummer S.A., 2000. “Detection of daytime sprites via a unique sprite ELF signature”. Geophys. Res. Lett., 27. doi: 10.1029/1999GL010769.

Stenbaek-Nielsen, H.C., Haaland, R., McHarg, M.G., Hensley, B.A., Kanmae T., 2010. Sprite initiation altitude measured by triangulation. J. Geophys. Res., 115, A00E12. doi:10.1029/2009JA014543.

Su, H.T., et al., 2003. Gigantic jets between a thundercloud and the ionosphere. Nature 423. doi:10.1038/nature01759.

Sukhorukov, A.I., Stubbe P., 1997. On ELF pulses from remote lightning triggering sprites, Geophys. Res. Lett., 24, 1639-1642.

van der Velde, O.A., 2008. Morphology of sprites and conditions of sprite and jet production in mesoscale thunderstorm systems. PhD thesis, University Paul Sabatier, Toulouse.

van der Velde, O.A., Mika, Á., Soula, S., Haldoupis, C., Neubert, T., Inan, U.S., 2006. Observations of the relationship between sprite morphology and in-cloud lightning processes. J. Geophys. Res., 111, D15203. doi:10.1029/2005JD006879.

van der Velde, O.A., Montanyà, J., Soula, S., Pineda, N., Bech, J., 2010. Spatial and temporal evolution of horizontally extensive lightning discharges associated with sprite-producing positive cloud-to-ground flashes in northeastern Spain. J. Geophys. Res., 115, A00E56. doi:10.1029/2009JA014773.

Wescott, E.M., Stenbaek-Nielsen, H.C., Sentman, D.D., Heavner, M.J., Moudry, D.R., São Sabbas, F.T.S., 2001. Triangulation of sprites, associated halos and their possible relation to causative lightning and micrometeors. J. Geophys. Res., 106, 10,467-10,477.

Williams, E.R., Mushtak, V.C., Boldi, R., Dowden, R.L., Kawasaki, Z.I., 2007. Sprite lightning heard round the world by Schumann resonance methods. Radio Sci. 42, RS2S20. doi:10.1029/2006RS003498.

Williams, E.R., Lyons, W.A., Hobara, Y., Mushtak, V.C., et al., 2010. Ground-based detection

of sprites and their parent lightning flashes over Africa during the 2006 AMMA campaign. Quart. J. Roy. Meteor. Soc., 136. dOI: 10.1002/qj.489.

Yair, Y., Price, C., Ganot, M., Greenberg, E., Yaniv, R., Ziv, B., Sherez, Y., Devir, A., Bór, J., Sátori, G., 2009. Optical observations of transient luminous events associated with winter thunderstorms near the coast of Israel. Atmos. Res., 91. doi:10.1016/j.atmosres.2008.06.018.

Table 1. Characteristics of the 17 TLE events: time and type of the TLE; time, distance from the camera at Pic du Midi, peak current and CMC of the associated P+CG stroke. IC means

intracloud.

Video	Event			P+CG stroke			
	#	Time (first frame) (UTC)	Type	Time* (UTC)	Distance (km)	Peak current (kA)	CMC (C km) ±20%
1	1	0209:56.599	column	.602	280	52.0	424
2	2	0233:16.686	column	.670	307	IC	
	3	0233:16.726	carrot	.738	360	32.9	
	4	0233:16.746	large carrot	.750	309	153.2	
	5	0233:16.966	column	.968	312	86.9	1049
3	6	0237:28.067	carrot	.067	312	195.8	
4	7	0241:17.108	column	.082	346	17.6	
	8	0241:17.188	large carrot	.202	303	70.1	1648
5	9	0246:40.830	column/carrot	.839	360	45.9	1464
6	10	0249:55.171	halo/column/carrot	.187	373	89.2	1199
	11	0249:55.451	carrot	.459	339	19.8	1332
7	12	0251:51.552	halo/carrot	.563	361	141.8	846
8	13	0256:15.213	column/carrot	.212	387	32.1	
	14	0256:15.513	undefined	.533	340	11.6	
9	15	0307:43.577	halo/column/carrot	.586	389	216.4	1678
	16	0307:43.737	carrot	.703	389	IC	
	17	0307:43.837	column/large carrot	.840	369	85.8	2088

* Time in second after the time of the first frame (column 3) in hour, minute and second (hhmm:ss).

Figure captions

Fig. 1. Geopotential at 500 hPa for September 1 at 0000 UT issued from the Global Forecast

System (GPS) model. The gray scale is in dam. The frames F_1 and F_2 represent the areas used in the areas used in other figures.

Fig. 2. Cloud top temperature from MSG satellite in F_1, at (a) 1825 UT on September 1, at (b) 0110 UT and (c) 0240 UT on September 2. Locations of -CG flashes (white crosses) and +CG flashes (red crosses) over 10 min around the time of the satellite scan are superimposed. The triangle indicates the camera location.

Fig. 3. CG flash density (km^{-2}) averaged over 5×5 km^2 during the whole storm lifetime in F_1 and in F_2 (see Fig. 1). The squares indicate the location of the P+CG flashes and the triangle indicates the camera location.

Fig. 4. Time series of: (a) minimum temperature of the cloud top, cloud area for several ranges of cloud top temperatures, (b) rate for both polarities of CG lightning flashes and +CG proportion, (c) average peak current for both polarities of CG lightning flashes. The arrow indicates the period of sprite observation (~57 min).

Fig. 5. Frames for six separate sprite events: from left to right and from up to down, #4, #8, #11, #12, #15, and #17. The distance from the camera to the P+CG stroke is 310 km, 300 km, 340 km, 360 km, 390 km, and 370 km, respectively. The displayed vertical scale is valid at the distance of the P+CG strokes. The time is indicated at the bottom of the frame as follows: hh:mm:ss; beginning and/or end of the frame (ms); frame number from the beginning of the GPS start-up.

Fig. 6. Time series of the peak current of the CG lightning flashes produced by the storm between 1700 UT (01/09) and 0500 UT (02/09). The triangles correspond to the 15 P+CG flashes.

Fig. 7. (a) Precipitation rate averaged over circles of 5 km radius around each CG flash versus peak current of the CG flash. (b) Difference in average precipitation rate between the circles

of 5 and 10 km radius around each CG flash versus peak current of the CG flash. The triangles correspond to the 15 P+CG flashes. CG flashes detected during the period 2200-0400 UT are considered.

Fig. 8. (a) Four successive frames during the sprite events at 2h 33min 16s. The line d_{1-4} corresponds with the lines of sight of different elements of the sprite events. (b) Chronology of the sequence including the peak current of the strokes (red triangle) and the video frames shown in (a). (c) Variation of the electric field radiated in ELF range (lower graph), VLF range (middle graph) and in LF (upper graph), detected at 1280 km in Bath (UK). (t=0 corresponds with the second P+CG parent stroke (2) detected at 2h 33min 16.750s). (d) Radar reflectivity field in F_2 at 0235 UT including the sprite lines of sight (d_{1-4}) and the P+CG strokes (red triangle).

Fig. 9. (a) Three frames during the sprite events at 2h 41min 17s. The line d_{1-3} corresponds with the lines of sight of different elements of the sprite event. (b) Chronology of the sequence including the peak current (red triangle) and the CMC (red dot with error bar) of the strokes, and the video frames shown in (a). (c) Variation of the electric field radiated in VLF range (upper graph) and in ELF range (middle graph) detected at 500 km in CEA station. (t=0 corresponds with the P+CG parent stroke detection at 2h 41min 17.202s). Lower graph: spectrum of the electric field radiated in broad band (ELF to LF). (d) Radar reflectivity field in F_2 at 0240 UT including the sprite lines of sight (d_{1-3}), the P+CG strokes (red triangle) and one -CG stroke (black triangle).

Fig. 10. (a) Four frames during the sprite event at 3h 07min 43s. The line d_{1-3} corresponds with the lines of sight of different elements of the sprite event. (b) Chronology of the sequence including the peak current (red triangle) and the CMC (red dot with error bar) of the strokes, and the video frames shown in (a). (c) Variation of the electric field radiated in ELF range (lower graph), VLF range (middle graph) and in LF (upper graph), detected at 1280 km in Bath (UK). (t=0 corresponds with the P+CG parent stroke detection at 3h 07min 43.586s (left) and at 3h 07min 43.840s (right). (d) Radar reflectivity field in F_2 at 0310 UT including

the sprite lines of sight ($d_{1\text{-}3}$) and the P+CG strokes (red triangle).

Fig. 11. (a) Sprite events geographic locations (colored circles) within the storm area and the transmitter-receiver paths (direct in solid line and scattered in dotted line). (b) VLF signals perturbations associated with the TLEs events and recorded by the receiver in Algiers.

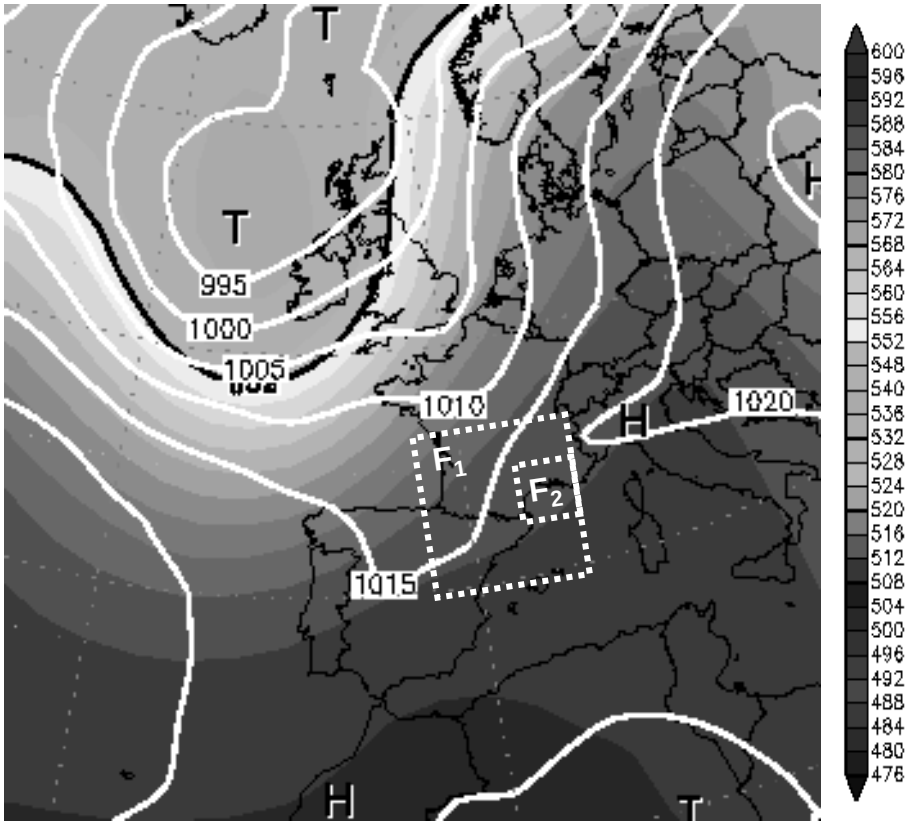
T
T
995
1000
1005
1010
H
1020
F1
F2
1015
H
T
H
600
596
592
588
584
580
576
572
568
564
560
556
552
548
544
540
536
532
528
524
520
516
512
508
504
500
496
492
488
484
480
476

Figure 1

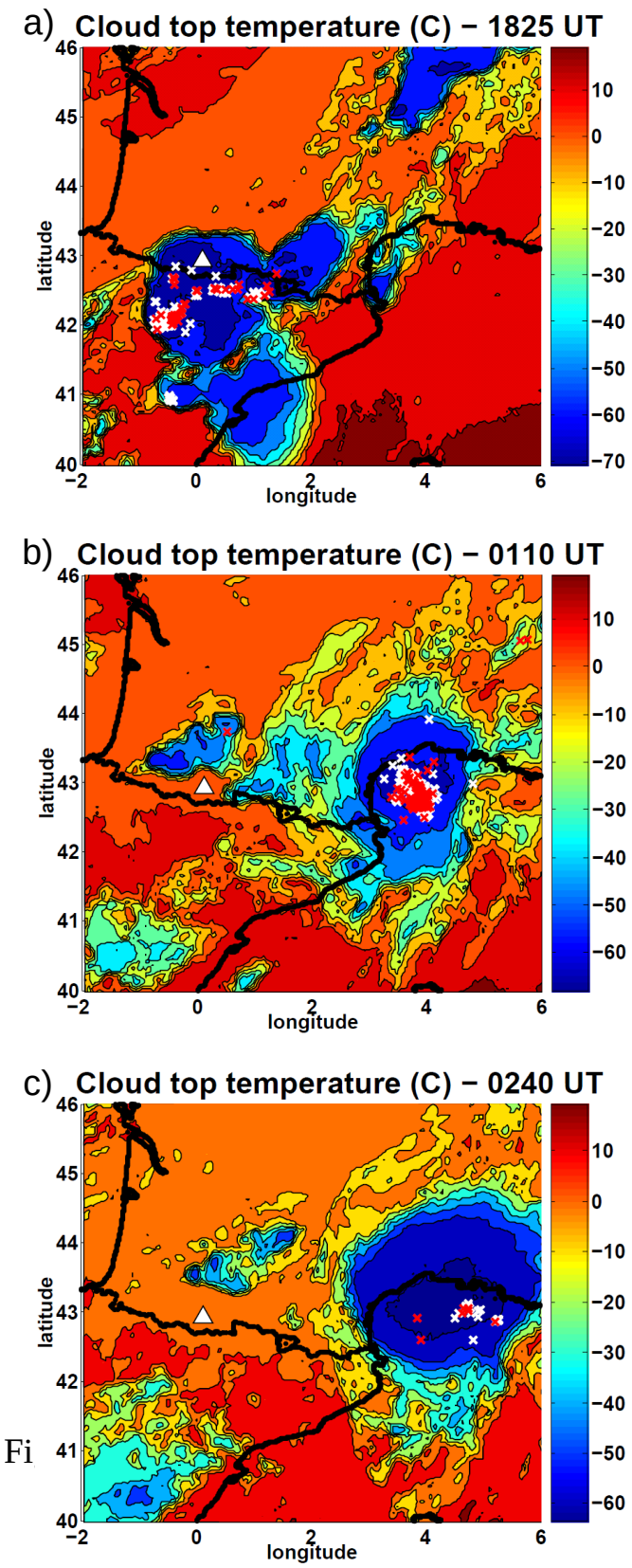
a) Cloud top temperature (C) − 1825 UT
b) Cloud top temperature (C) − 0110 UT
c) Cloud top temperature (C) − 0240 UT
latitude
longitude
46
45
44
43
42
41
40
−2
0
2
4
6
10
0
−10
−20
−30
−40
−50
−60
−70

Fi

Figure 2

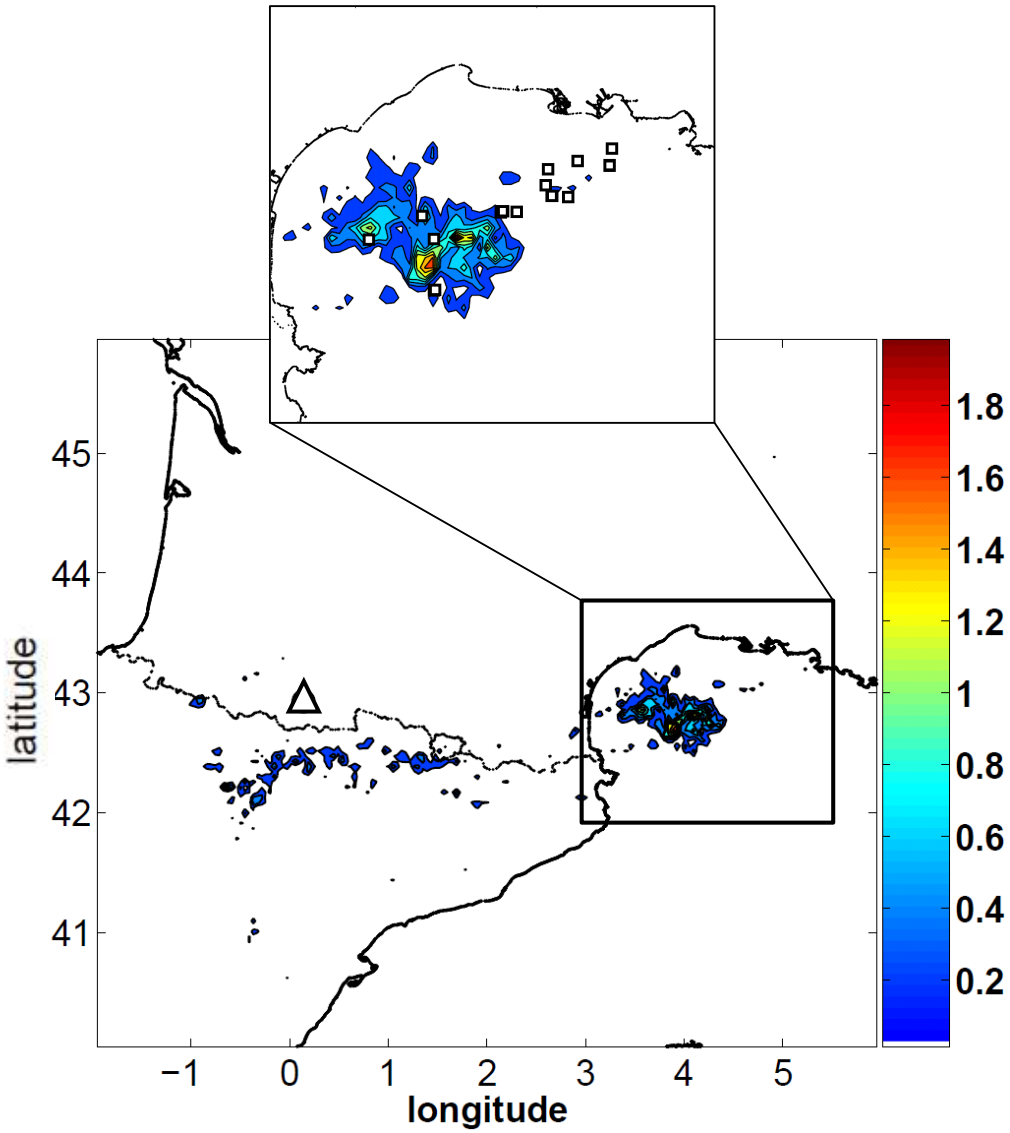
45
44
43
42
41
latitude
−1
0
1
2
3
4
5
longitude
1.8
1.6
1.4
1.2
1
0.8
0.6
0.4
0.2

Figure 3

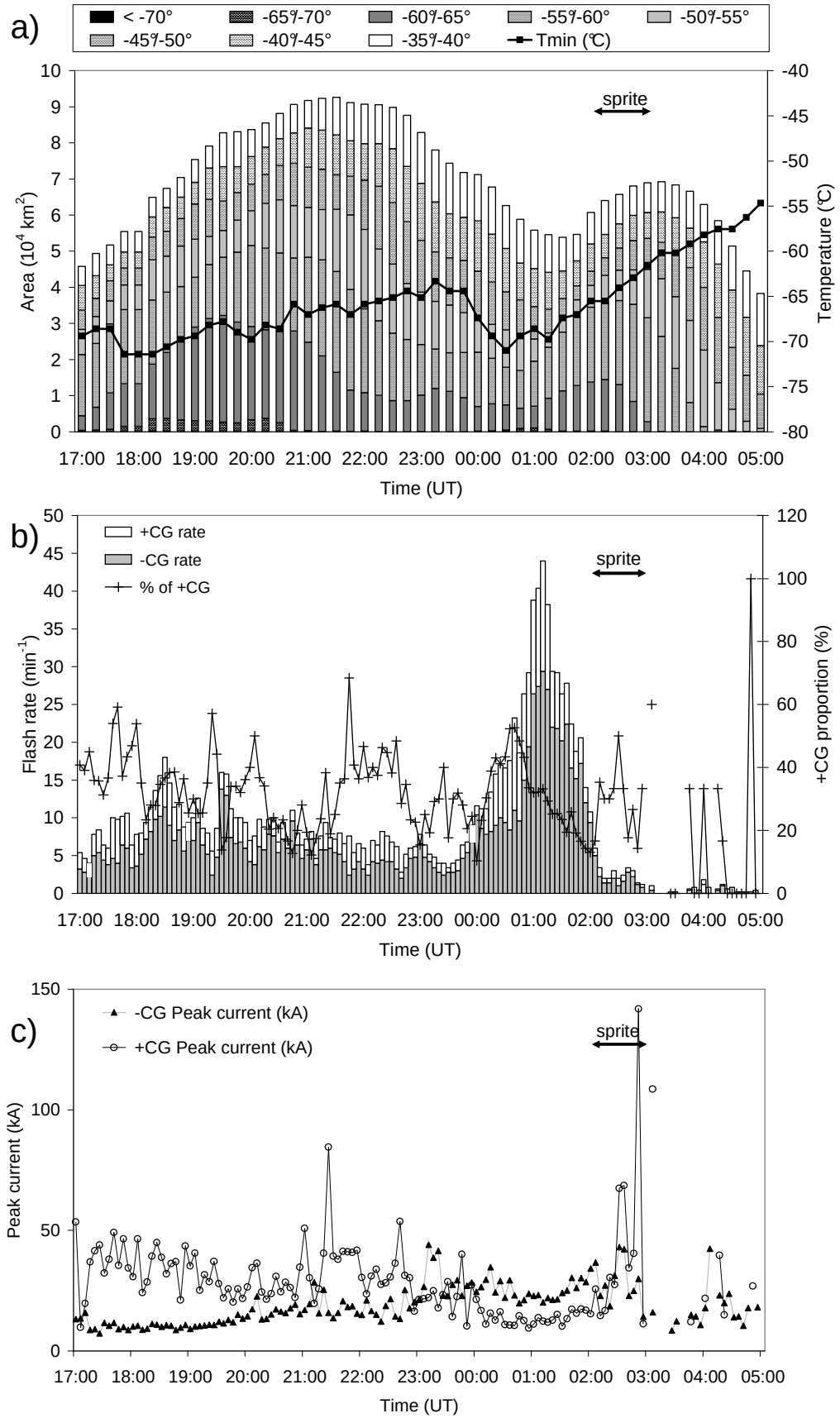
a)
< -70°
-65°-70°
-60°-65°
-55°-60°
-50°-55°
-45°-50°
-40°-45°
-35°-40°
Tmin (℃)
sprite
Area (10^4 km^2)
Temperature (℃)
Time (UT)
b)
+CG rate
-CG rate
% of +CG
sprite
Flash rate (min^{-1})
+CG proportion (%)
Time (UT)
c)
-CG Peak current (kA)
+CG Peak current (kA)
sprite
Peak current (kA)
Time (UT)

Figure 4

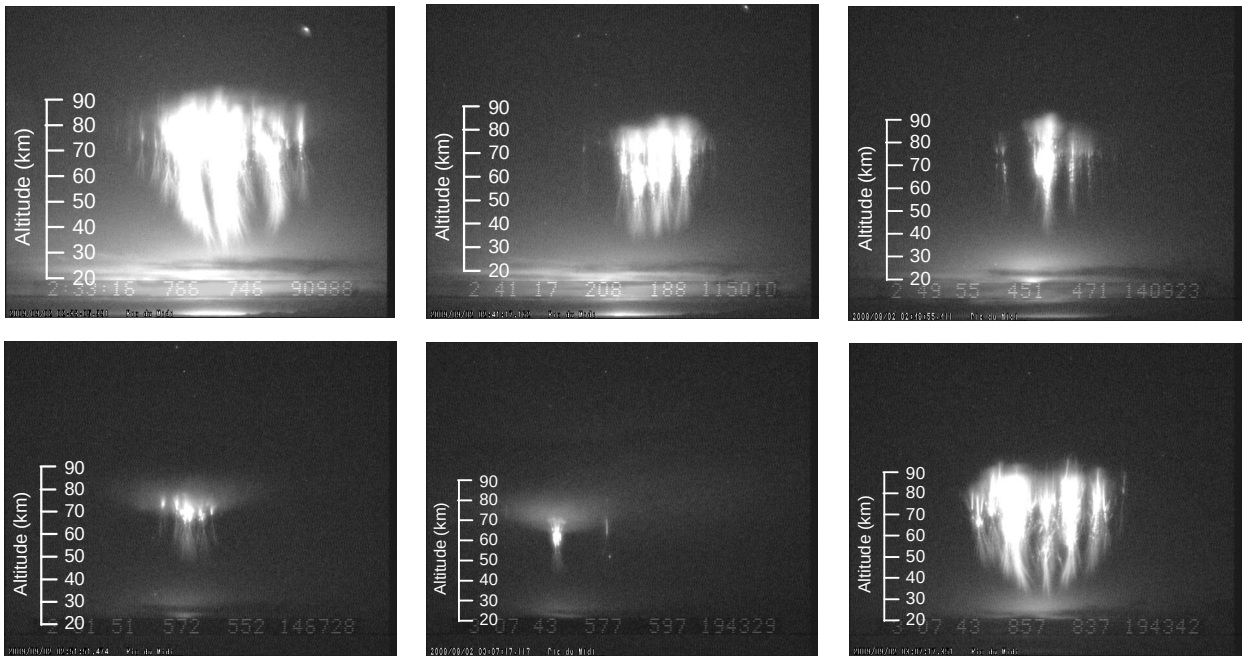

Figure 5

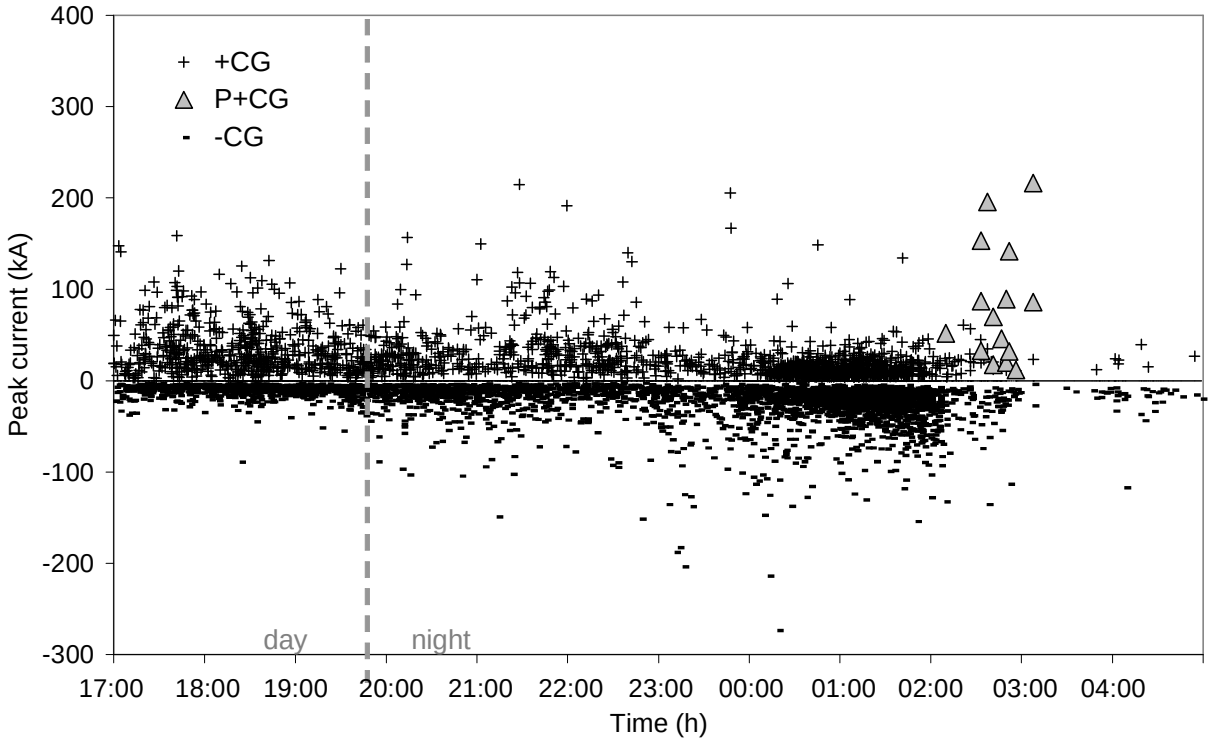
+CG
P+CG
-CG
Peak current (kA)
400
300
200
100
0
-100
-200
-300
day
night
17:00
18:00
19:00
20:00
21:00
22:00
23:00
00:00
01:00
02:00
03:00
04:00
Time (h)

Figure 6

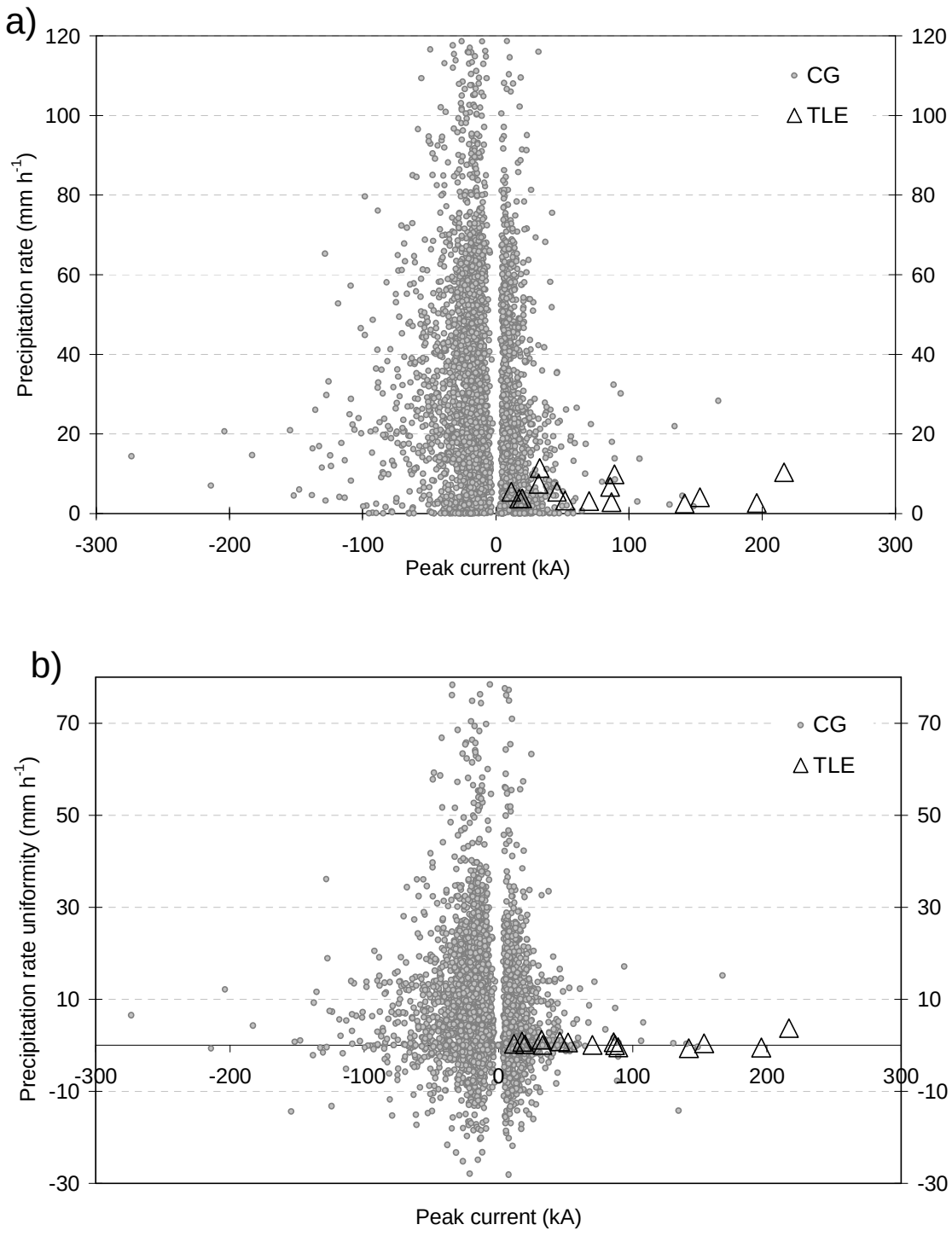
a)
Precipitation rate (mm h-1)
Peak current (kA)
CG
TLE
b)
Precipitation rate uniformity (mm h-1)
Peak current (kA)
CG
TLE

Figure 7

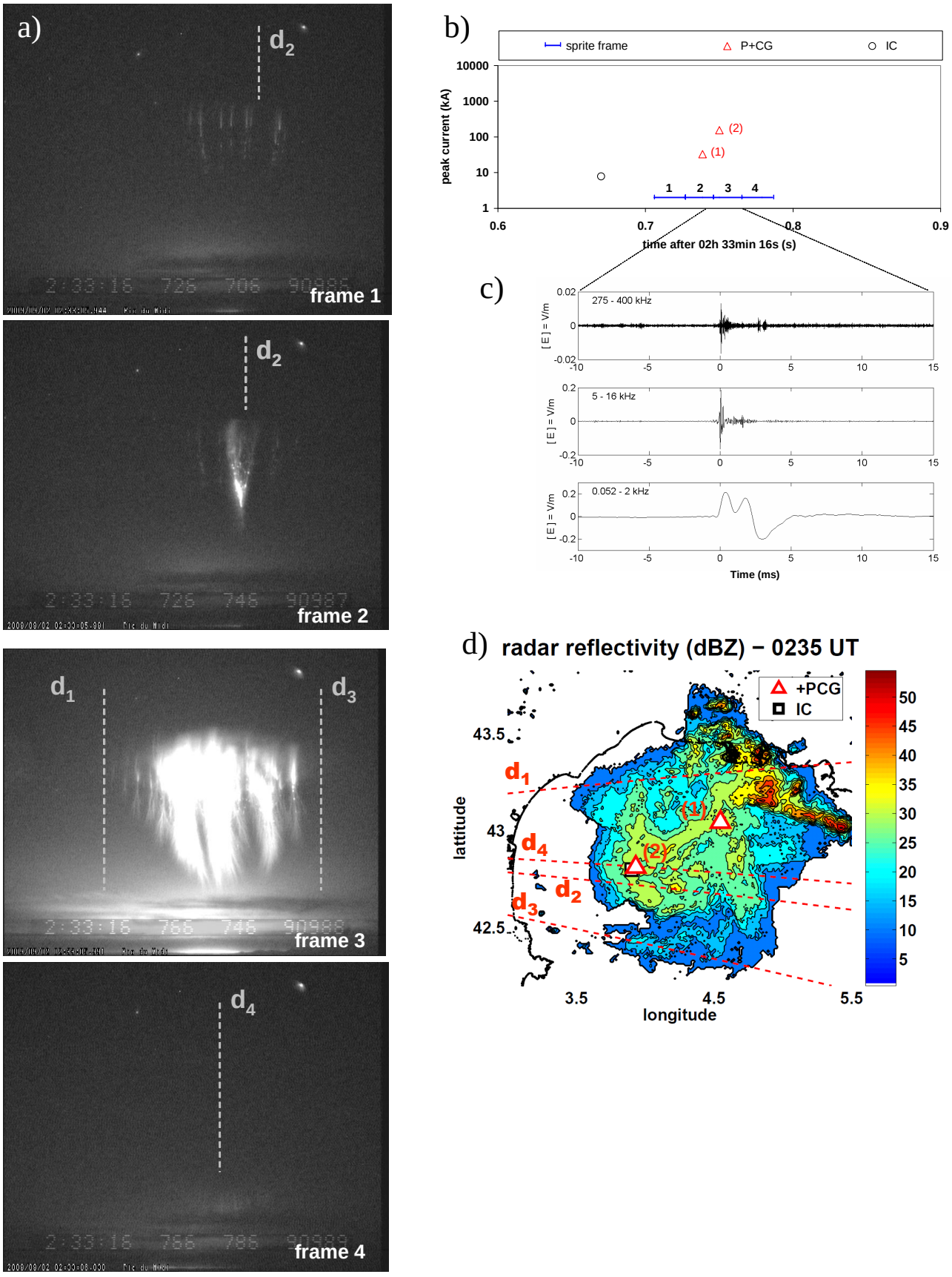
a)
d2
frame 1
d2
frame 2
d1
d3
frame 3
d4
frame 4
b)
sprite frame
P+CG
IC
peak current (kA)
10000
1000
100
10
1
(2)
(1)
1
2
3
4
0.6
0.7
0.8
0.9
time after 02h 33min 16s (s)
c)
275 - 400 kHz
5 - 16 kHz
0.052 - 2 kHz
[E] = V/m
Time (ms)
d) radar reflectivity (dBZ) − 0235 UT
+PCG
IC
43.5
43
42.5
lattitude
d1
d2
d3
d4
(1)
(2)
3.5
4.5
5.5
longitude
50
45
40
35
30
25
20
15
10
5

Figure 8

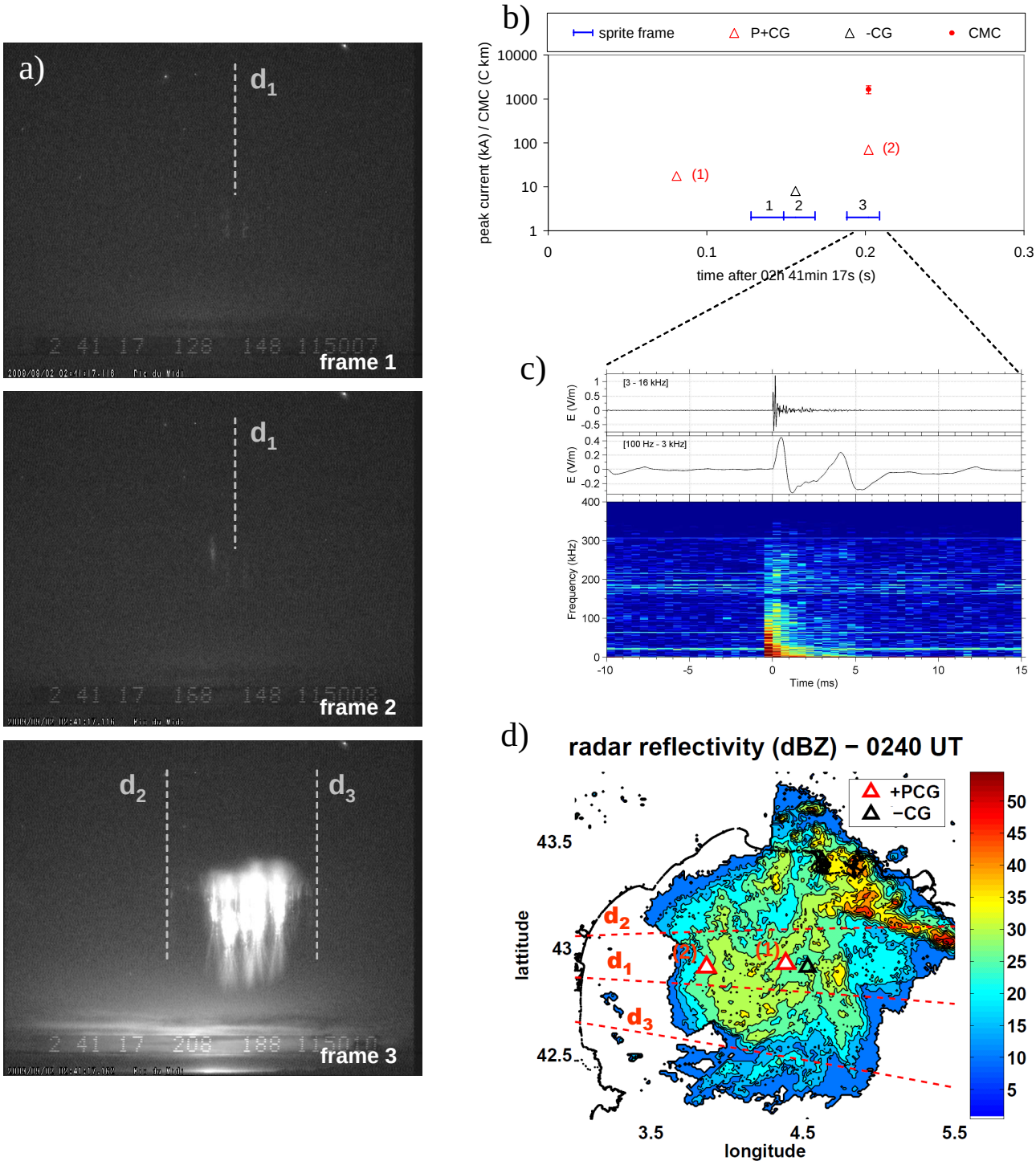
a)
d1
frame 1
d1
frame 2
d2
d3
frame 3
b)
sprite frame
P+CG
-CG
CMC
peak current (kA) / CMC (C km)
10000
1000
100
10
1
(1)
(2)
1
2
3
0
0.1
0.2
0.3
time after 02h 41min 17s (s)
c)
[3 - 16 kHz]
E (V/m)
[100 Hz - 3 kHz]
E (V/m)
Frequency (kHz)
400
300
200
100
0
-10
-5
0
5
10
15
Time (ms)
d)
radar reflectivity (dBZ) − 0240 UT
+PCG
−CG
43.5
43
42.5
lattitude
d2
d1
d3
(2)
(1)
3.5
4.5
5.5
longitude
50
45
40
35
30
25
20
15
10
5

Figure 9

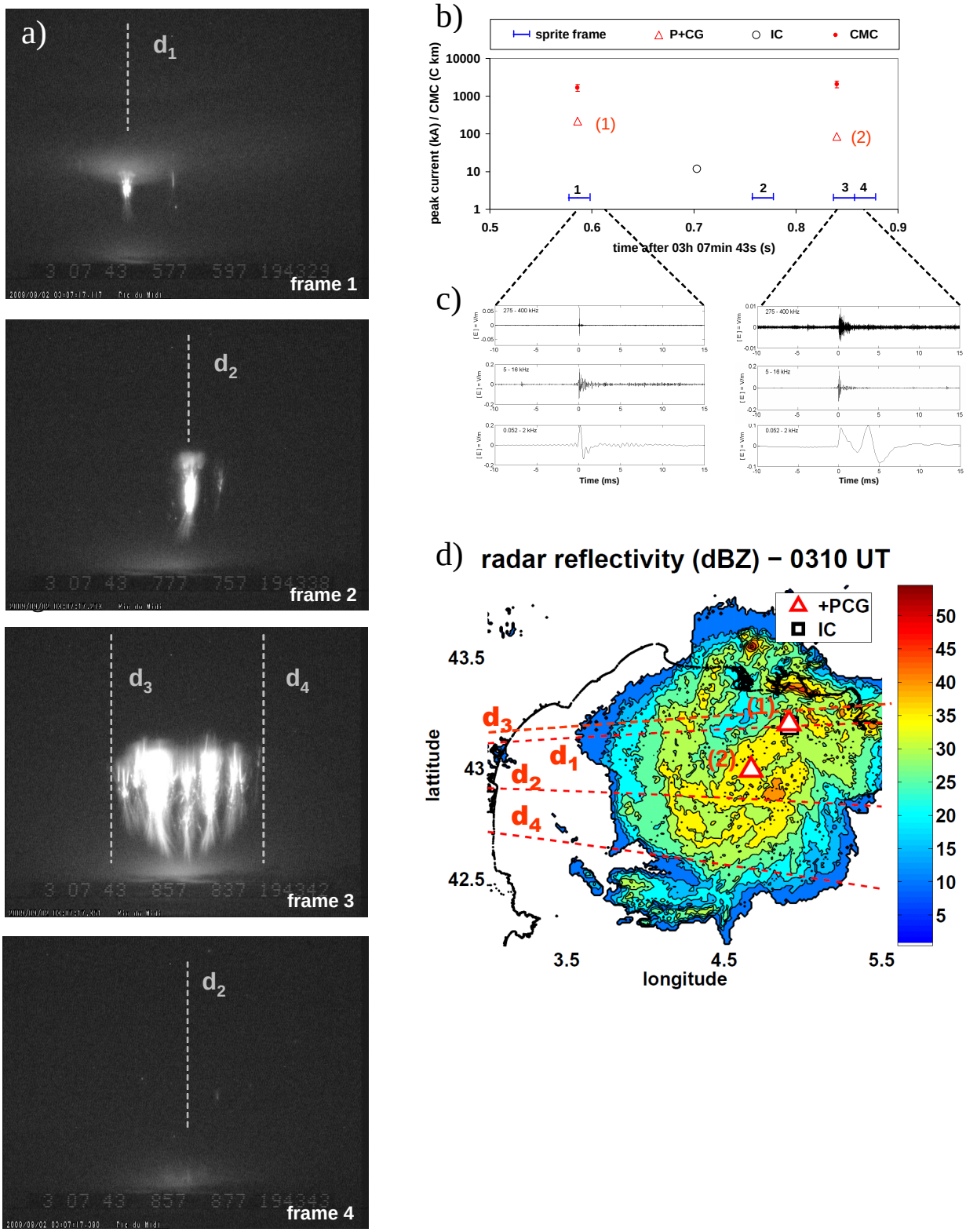
a)
d1
frame 1
d2
frame 2
d3
d4
frame 3
d2
frame 4
b)
sprite frame
P+CG
IC
CMC
peak current (kA) / CMC (C km)
10000
1000
100
10
1
(1)
(2)
1
2
3
4
0.5
0.6
0.7
0.8
0.9
time after 03h 07min 43s (s)
c)
275 - 400 kHz
5 - 16 kHz
0.052 - 2 kHz
Time (ms)
d) radar reflectivity (dBZ) − 0310 UT
+PCG
IC
43.5
43
42.5
lattitude
3.5
4.5
5.5
longitude
d1
d2
d3
d4
(1)
(2)
50
45
40
35
30
25
20
15
10
5

Figure 10

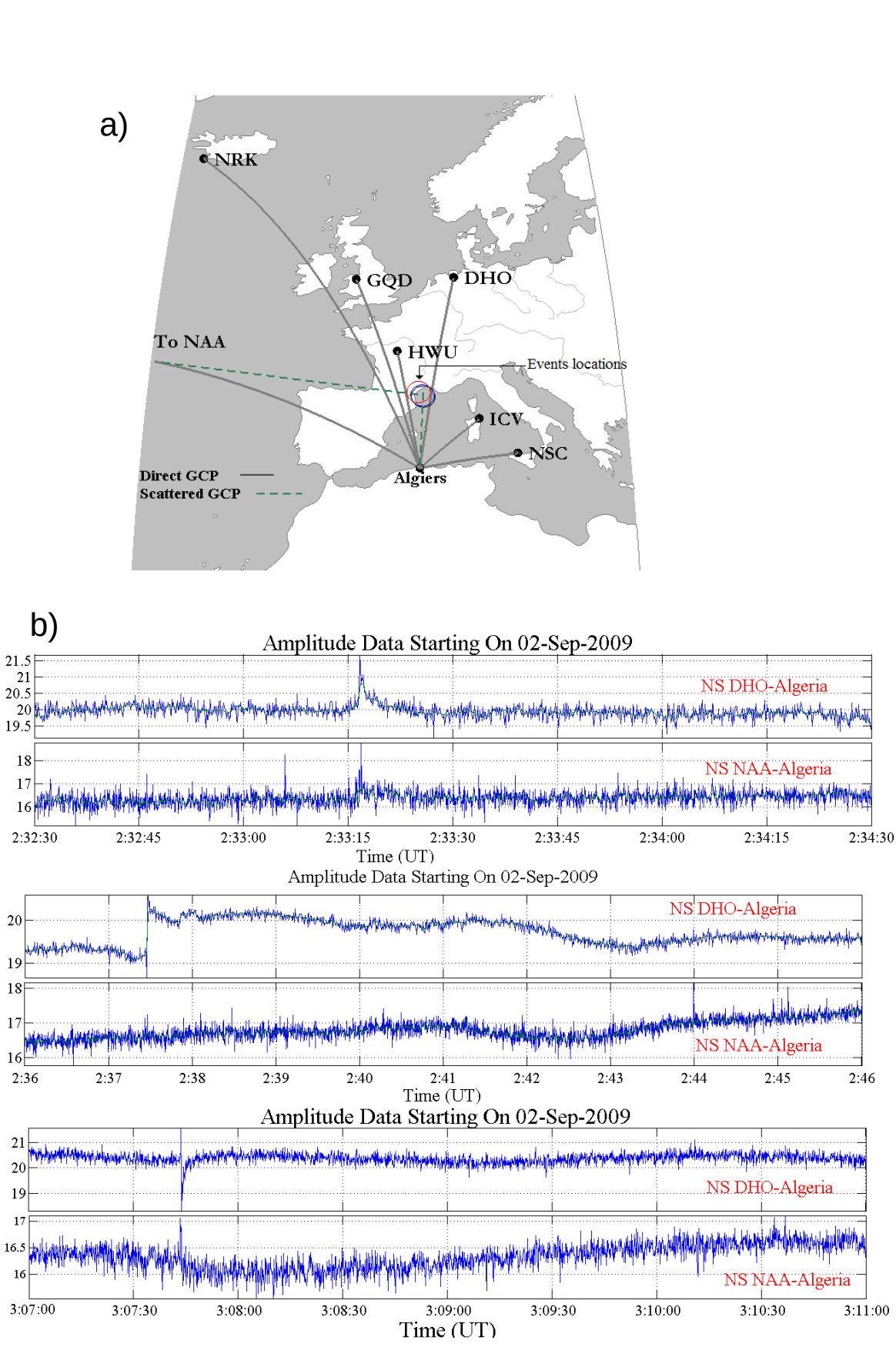
a)
NRK
GQD
DHO
To NAA
HWU
Events locations
ICV
NSC
Algiers
Direct GCP
Scattered GCP
b)
Amplitude Data Starting On 02-Sep-2009
NS DHO-Algeria
NS NAA-Algeria
Time (UT)
Amplitude Data Starting On 02-Sep-2009
NS DHO-Algeria
NS NAA-Algeria
Time (UT)
Amplitude Data Starting On 02-Sep-2009
NS DHO-Algeria
NS NAA-Algeria
Time (UT)

Figure 11